ACS Biomaterials SCIENCE & ENGINEERING

pubs.acs.org/journal/abseba Article

High-Throughput and Continuous Chaotic Bioprinting of Spatially Controlled Bacterial Microcosms

Carlos Fernando Ceballos-González,[#] Edna Johana Bolívar-Monsalve,[#] Diego Alonso Quevedo-Moreno, Li Lu Lam-Aguilar, Karen Ixchel Borrayo-Montaño, Juan F. Yee-de León, Yu Shrike Zhang, Mario Moisés Alvarez,* and Grissel Trujillo-de Santiago*

Cite This: *ACS Biomater. Sci. Eng.* 2021, 7, 2408−2419 Read Online

ACCESS | Metrics & More | Article Recommendations | Supporting Information

ABSTRACT: Microorganisms do not work alone but instead function as collaborative microsocieties. The spatial distribution of different bacterial strains (micro-biogeography) in a shared volumetric space and their degree of intimacy greatly influences their societal behavior. Current microbiological techniques are commonly focused on the culture of well-mixed bacterial communities and fail to reproduce the micro-biogeography of polybacterial societies. Here, we bioprinted fine-scale bacterial microcosms using chaotic flows induced by a printhead containing a static mixer. This straightforward approach (i.e., continuous chaotic bacterial bioprinting) enables the fabrication of hydrogel constructs with intercalated layers of bacterial strains. These multilayered constructs are used to analyze how the spatial distributions of bacteria affect their social behavior. For example, we show that bacteria within these biological microsystems engage in either cooperation or competition, depending on the degree of shared interface. The extent of inhibition in predator−prey scenarios (i.e., probiotic−pathogen bacteria) increases when bacteria are in greater intimacy. Furthermore, two *Escherichia coli* strains exhibit competitive behavior in well-mixed microenvironments, whereas stable coexistence prevails for longer times in spatially structured communities. We anticipate that chaotic bioprinting will contribute to the development of a greater complexity of polybacterial microsystems, tissue-microbiota models, and biomanufactured materials.

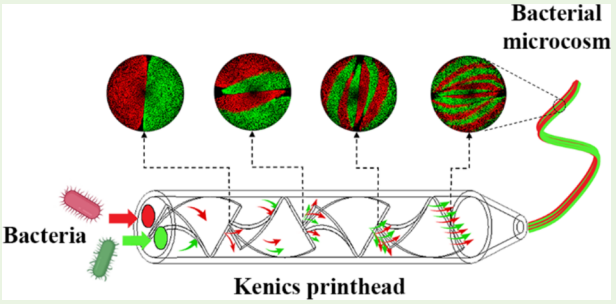

KEYWORDS: *bioprinting, Kenics, bacteria, chaotic, micro-biogeography*

INTRODUCTION

Microorganisms do not work alone but instead function in highly dynamic societies in which members collaborate and/or compete. A growing body of evidence demonstrates that the spatial distribution in microbial societies also matters.[1,2] Micro-biogeography, the spatial patterns of microbial communities through time and space,[3,4] greatly influences the dynamics of microbial ecosystems. In turn, the emergence of any particular microgeography depends on gradients in the local micro-environment (i.e., variations in temperature, oxygen concentration, pH, and nutrients)[5,6] that often are induced by the concerted acting of microorganisms.

This interplay between micro-biogeography and societal function has diverse examples in nature. For instance, in the plant kingdom, trees host microcommunities with structured micro-biogeographies, such as lung lichens made of bacteria, algae, and fungi. Associations of algae and bacteria have been observed in lichen cross sections, forming 30-μm-wide interspersed lamellae.[7] In biofilms, bacteria form aggregates made of mono- or polybacterial species that play distinct roles according to their phenotypes.[8,9] When bacteria at the periphery cause a depletion of available substrates at the interior, the inner cells starve and interrupt the synthesis of metabolites that are vital for their counterparts on the outside. This dynamic leads to spatiotemporal variations in the bacterial community.[10] Similarly, the distribution and composition of human microbiota vary across different body habitats.[11,12] In caries and periodontal pockets, mosaic architectures of biofilms emerge due to the presence of anaerobes in the interior and aero-tolerant taxa on the exterior, creating hedgehog, corncob, and cauliflower-like microstructures.[13,14] An improved understanding of microbiota organization on teeth, for example, may help in developing more efficient dental therapies.[15] In the gut, the micro-biogeography is also very complex and dynamic.[16] A large variety of symbiotic microorganisms coexist in digestive tract of mammals. Their interactions and their interplay with

Received: November 23, 2020
Accepted: April 28, 2021
Published: May 12, 2021

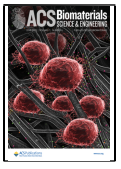

https://doi.org/10.1021/acsbiomaterials.0c01646
ACS Biomater. Sci. Eng. 2021, 7, 2408−2419

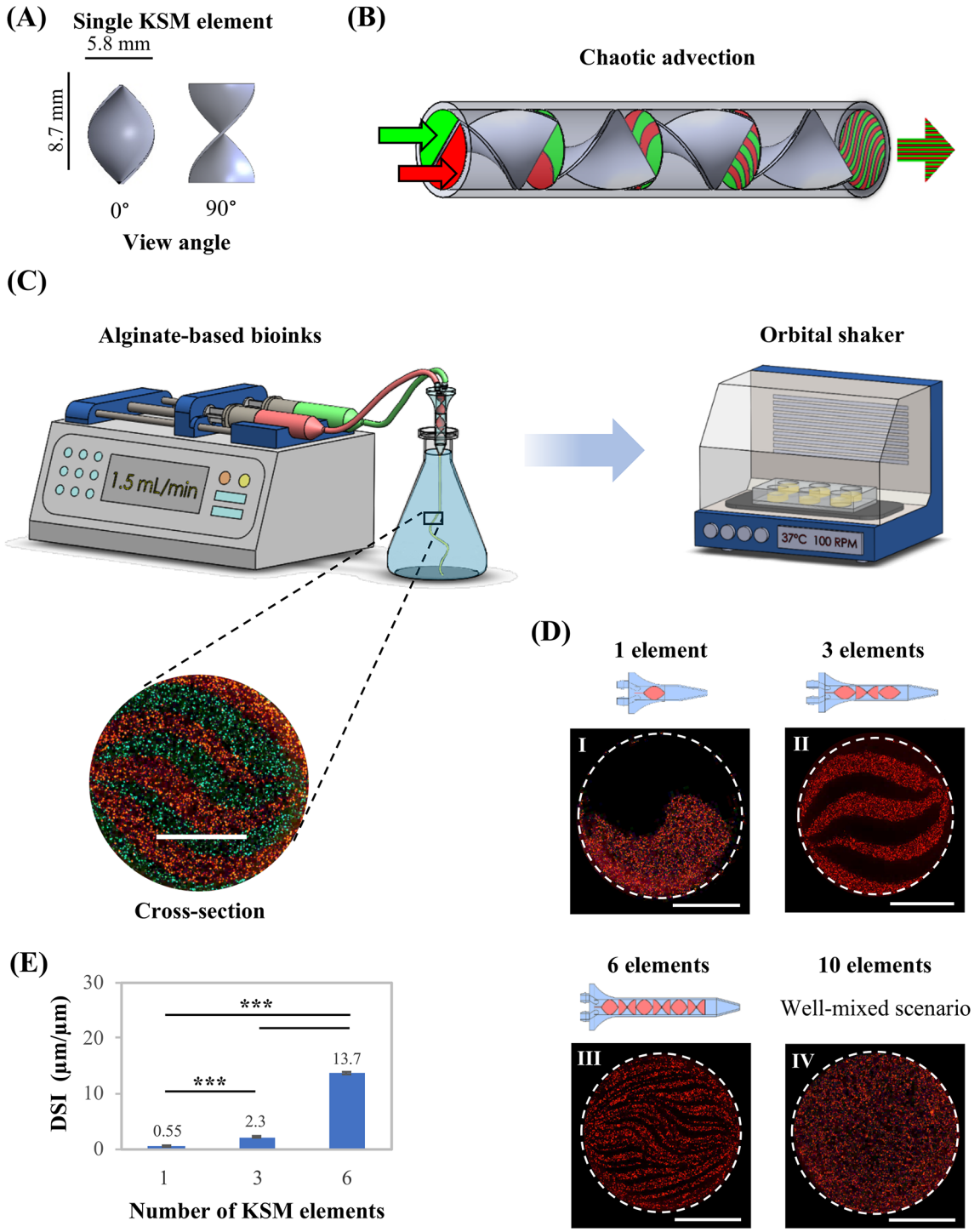

Figure 1. Continuous chaotic bioprinting of fine-scale micro-biogeographies. (A) A single KSM element seen from two view angles. (B) Illustration of a multilamellar pattern developed by the successive splitting and folding of bioinks at each mixing element. (C) Schematic diagram of the procedure for bioprinting and culture microcosms-containing fibers using a printhead equipped with 3-KSM elements. The outlet of the KSM printhead must be immersed in the calcium chloride ($CaCl_2$) solution. A cross-section of a printed fiber is shown. Scale bar: 500 μm. (D) Printheads containing different numbers of KSM elements and representative micrographs of the micro-biogeographies produced. (E) Quantification of the DSI at each micro-biogeography. ***p-value < 0.001 (n = 3).

host cells play a crucial role in health and disease. However, the microbiota is not "well-mixed" but stratified and segregated to accomplish complex societal functions.[17,18]

Among the many factors that govern the degree of interaction between different organisms in a bacterial society, the extent of segregation or mixing and the degree of shared interface has proven to be highly relevant.[19−21] Nevertheless, conventional microbiological culture techniques fail to generate these complex microarchitectures of bacteria and substrates, thereby limiting the study of the effects of spatial variations on the societal dynamics of microbial communities.[19,20] One strategy to address this issue is to use

https://doi.org/10.1021/acsbiomaterials.0c01646
ACS Biomater. Sci. Eng. 2021, 7, 2408−2419

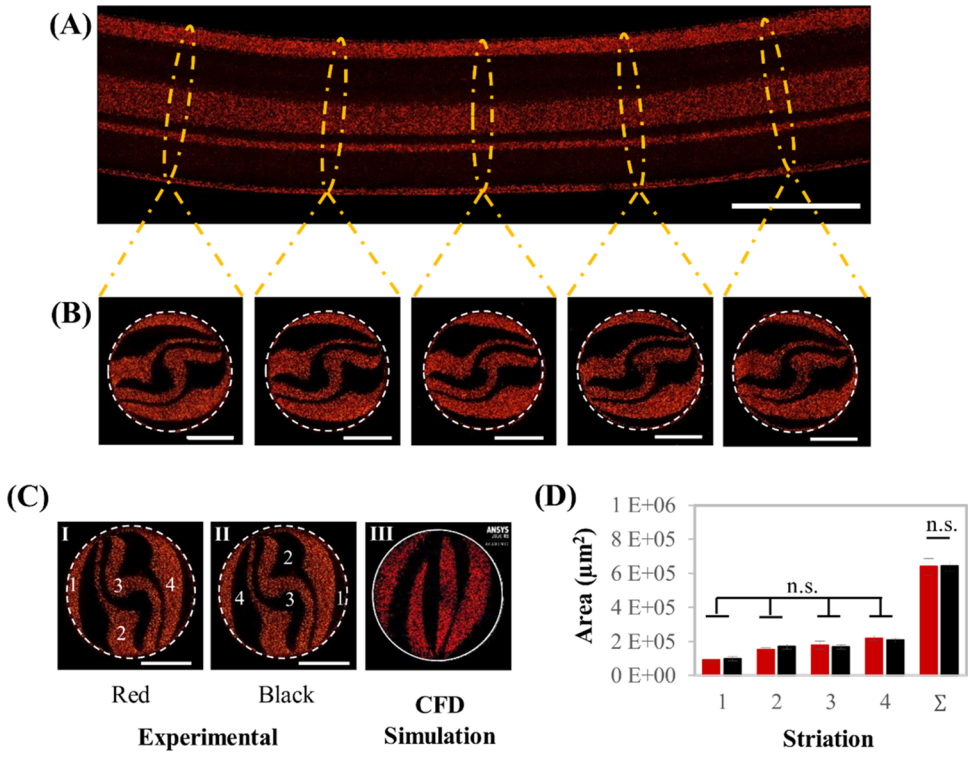

Figure 2. Reproducibility and throughput of the lamellar microstructure. (A) Axial view of a fiber printed using three KSM elements. Scale bar: 1000 μm. (B) Cross-sectional cuts of the same fiber at different lengths exhibit a conserved multilamellar pattern. Scale bar: 500 μm. (C) Mirror-like projections of homologous lamellae marked by the same number (I and II), and CFD simulation of the cross-sectional microstructure after 3-KSM elements (III). (D) The individual and total (Σ) areas of red and black striations among seven cross-sectional cuts obtained experimentally. Nonsignificant difference (n.s.) at p-value < 0.05 (n = 7).

biofabrication techniques, such as bioprinting, micromolding, photolithography patterning, and microfluidics-based manufacturing in microbiology. Hynes et al.[22] accommodated spatially distinct aggregates of *Escherichia coli* and *Salmonella enterica* using a casting-based method and suggested that interactions in this consortium may be influenced by spatial scales. Similarly, Chen et al.[23] used photolithography to create patterns in adhesion polymers at a resolution of 10 μm. The patterns were subsequently used for specific anchoring of *E. coli* at those locations, and the authors then monitored bacterial crosstalk using a reporter gene activated by the high cell concentration in neighboring fronts. Qian et al.[24] used an extrusion-based system to print diverse 3D geometries with a 200 μm resolution for biomanufacturing purposes. Lattice-shaped scaffolds containing *Saccharomyces cerevisiae* were capable of a continuous synthesis of ethanol not possible when these organisms were cultured in solid layers. This difference presumably arose because the porosity of the latticed scaffolds facilitated mass transfer. However, often these technologies demand sophisticated equipment, are labor intensive, require technical expertise to be built or operated, or exhibit a modest throughput.

In this contribution, we show that continuous chaotic bioprinting[25,26] is a versatile, cost-effective, user-friendly, and high-throughput microbiology tool for creating bacterial microsystems with a printing resolution of a few tens of micrometers. In addition, we show that our printed microcosms are alive, and dynamic eco-systems respond to the printed micro-biogeography; the degree of shared interface between two distinct microbial communities greatly matters to determine the dynamics of competition in the entire microsystem. We first demonstrate that bacterial viability inhibition is strongly influenced by the degree of intimacy between two distinct bacterial strains. We then show that even cells from the same species may exhibit competition, depending on their spatial distribution.

RESULTS AND DISCUSSION

Characterization of Spatial Distribution. Chaotic advection, defined as the continuous stretching and folding of materials that yield a chaotic flow, is extensively used in industrial mixing when turbulence is either unfeasible or inappropriate.[27−29] Chaotic advection can be induced by, for example, a Kenics static mixer (KSM),[29] which is an arrangement of motionless helicoidal mixing elements (Figure 1A) fixed in a cylindrical housing.

Recently, our group reported the first use of chaotic flows produced within a KSM for the continuous chaotic bioprinting of spatially organized cells at both high throughput (>1 m·min^{-1}) and high resolution (~10 μm).[25,26] Extrusion of two bioinks through a printhead containing a KSM increases the number of interfaces between them exponentially according to the number of mixing elements used (Figure 1B). The printing resolution of our technique, in terms of the thickness of the internal lamellae, can be simply tuned by changing the number of KSM elements in the printhead. In addition, the number of lamellae generated can be calculated according to the model $s = 2^n$, where s is the number of lamellae and n is the number of KSM elements.

Here, we use continuous chaotic bioprinting to enable a precise accommodation of bacterial communities in fine-scale multilamellar structures. These bioprinted constructs were

https://doi.org/10.1021/acsbiomaterials.0c01646
ACS Biomater. Sci. Eng. 2021, 7, 2408−2419

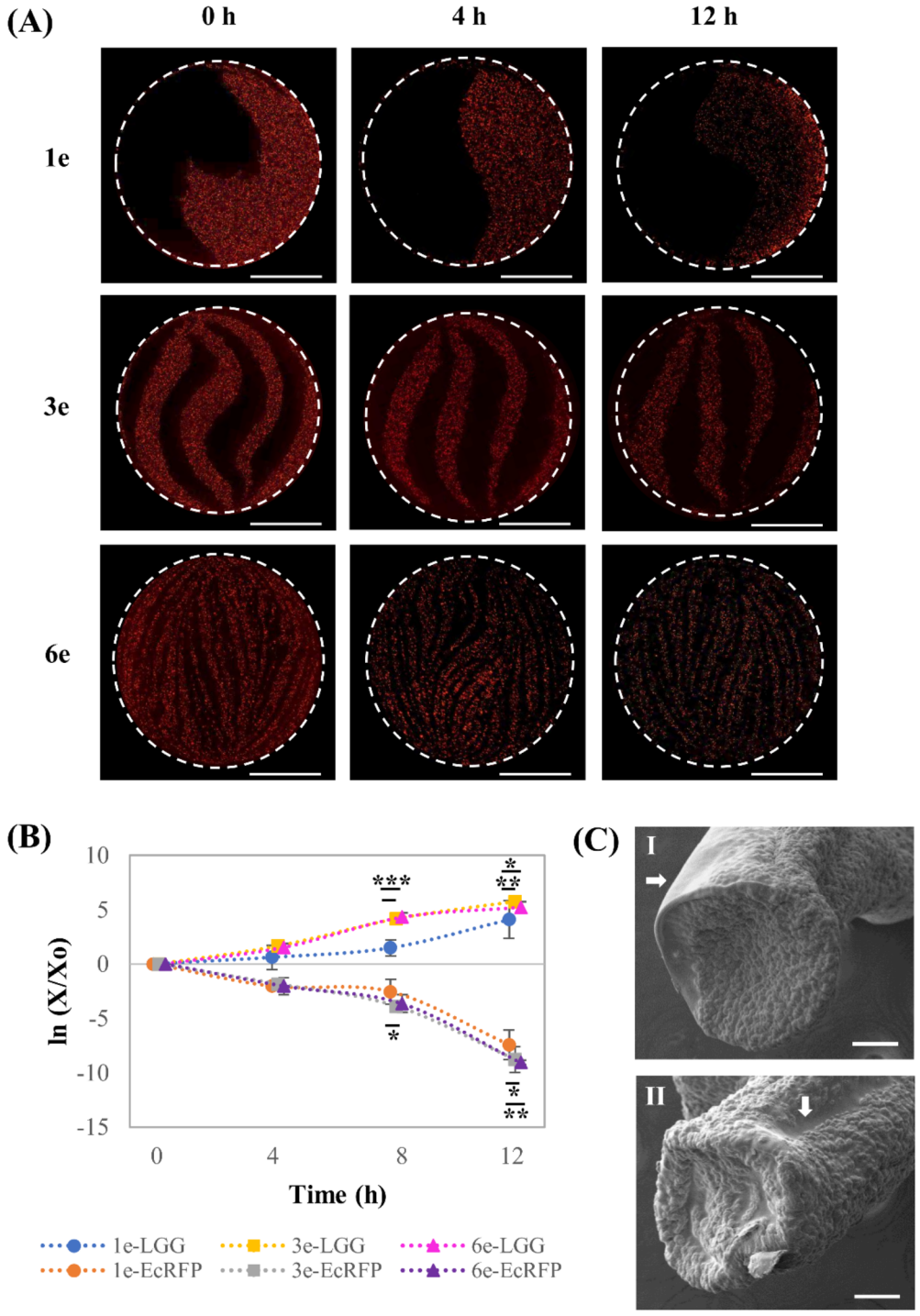

Figure 3. Dynamics of the inhibition of *Escherichia coli* by *Lactobacillus rhamnosus* GG. (A) Cross-section of the micro-biogeographies containing RFP-expressing *E. coli* (EcRFP; red) and LGG (black), chaotically printed using 1-, 3-, or 6-KSM elements (scale bar: 500 μm). (B) Coculture viability over a 12 h duration, normalized by the number of colony-forming units (CFUs) just after bioprinting. (C) SEM micrographs showing the invasion of EcRFP neighborhoods by LGG, in constructs printed using 1- (I) and 3- (II) KSM elements. *p-value < 0.05; **p-value < 0.001; ***p-value < 0.001 (n = 6).

then used to assess the impact of the degree of intimacy between bacterial microclusters on their social behavior, as evaluated in terms of cell-viability (viable cell counts). Our simple printing setup consisted of a KSM printhead, the bioinks, a syringe pump, and a 2% $CaCl_2$bath (Figure 1C). This system enables the high-throughput fabrication of fiber-shaped scaffolds 1 mm in diameter and containing striations as large as 500 μm or as small as 7 μm (Figure 1D). We first characterized the spatial distribution of our bacterial microcosms. To do this, we coextruded a suspension of red fluorescent bacteria in pristine alginate ink (2% w/v) with a nonfluorescent pristine alginate ink (2% w/v). The tight hydrogel mesh provided by the alginate hydrogel (pore size values lower than 1 μm)[30,31] constrains bacteria in the position

https://doi.org/10.1021/acsbiomaterials.0c01646
ACS Biomater. Sci. Eng. 2021, 7, 2408−2419

at which they are initially bioprinted. This suggests that the social behaviors observed in our bioprinted constructs arise as a consequence of the interaction through solutes diffused in media and their local concentrations.

Overall, we chaotically printed four different micro-biogeographies: printheads equipped with 1-, 3-, 6-, or 10-KSM elements produced constructs containing 2, 8, 64, and 1024 defined lamellae and a homogeneous microcosm, respectively (Figure 1D). In principle, the 10-KSM element printhead would render 1024 lamellae of 0.97 μm-thickness accommodated in a fiber of 1 mm diameter. In this particular setup, the size of the bacteria (approximately 2 μm), which was larger than the average size of the striations, prevented the generation of a layered microstructure.[32]

We then established the degree of shared interface (DSI) as a quantitative descriptor of intimacy between bacterial striations (Figure 1E). The rationale behind the use of DSI arises from the fact that the intermaterial interface is exponentially incremented by chaotic advection.[25,33] The DSI was expressed as the ratio of the total length of the boundaries between lamellae and the fiber perimeter (Equation 1). Figure 1E shows that printheads equipped with 1-, 3-, or 6-KSM elements generate a DSI of 0.55, 2.3, or 13.7 μm/μm, respectively.

$$\text{DSI} = \frac{\text{Total length of the boundaries between striations } (\mu\text{m})}{\text{perimeter of the cross section } (\mu\text{m})} \quad (1)$$

Subsequently, we analyzed the reproducibility of the lamellar microstructure along a printed fiber (Figure 2A). Figure 2B shows cross-sectional cuts from the same scaffold at different distances and confirms that the striation pattern is highly conserved throughout the whole fiber and that each red lamella (Figure 2C, I) had an identical black counterpart (Figure 2C, II) in the same cross-section. This phenomenon can be explained in terms of the self-similar nature of chaotic flows, that is, the repetitive iteration on the same flow manifold throughout n number of stretching and folding cycles.[32,33] This self-similarity between lamellae was also evident in simulation results obtained using computational fluid dynamics (CFD) strategies to solve the Navier−Stoke equations of fluid motion (Figure 2C, III).[29] We then analyzed a series of cross sections along the fiber and calculated the individual area of homologous lamellae and the cumulative area of the black and red lamellae (Figure 2D). We found that the area of the analogous lamellae, (i.e., the symmetric black and red lamellae in the same cross section) is practically equivalent. The areas of analogous lamellae at different cross sections were also equivalent (variance coefficient from 6 to 14%; Supplementary Table 1). The projected cumulative area of the black and red regions at each cross section was significantly similar. This implies that both inks occupy the same amount of territory (surface) in the scaffold; therefore, our bacterial strains would be equally distributed when contained in a chaotically printed micro-biogeography.

***E. coli* versus *Lactobacillus rhamnosus* GG.** Communication and/or synchronized behavior in bacterial communities are often conceived as phenomena that mainly depend on the cell density and diversity of the species within the community.[23,34] However, a growing body of evidence suggests a paramount role as well for spatial positioning in bacterial societal behavior.[1,3,35−37]

In our first biological scenario, a recombinant *E. coli* strain, engineered to produce a red fluorescent protein (EcRFP), and a nonrecombinant *L. rhamnosus* GG (LGG) were used for modeling a simplified probiotic−pathogen interplay. LGG is a probiotic thought to suppress overgrowth of pathogenic gut bacteria through diverse mechanisms including interference with pathogen adhesion, secretion of antibacterial compounds (i.e., lactic acid, antibacterial peptides, etc.), and stimulation of the host immune response.[38,39]

Prior to the bioprinting process, both bacteria were cultivated for 24 h in fresh medium to achieve a maximum cell density. Each bacterial culture was then centrifuged and placed into a different reservoir containing a mixture of sodium alginate and culture medium. We ensured the reproducibility of our experiments by adjusting the initial cell density of our bioinks to an optical density (OD) at 600 nm of 0.1 and 0.025 for EcRFP and LGG, respectively. These ODs rendered nearly the same number of colony-forming units (CFUs) for each strain just after bioprinting (approximately 7.8×10^7 CFUs/mL). We printed micro-biogeographies using a printhead equipped with 1-, 3-, or 6-KSM elements. These bacterial constructs were cultivated over a 12 h duration at 100 rpm and 37 °C in a mixture of Luria−Bertani (LB) and de Man, Rogosa and Sharpe (MRS) media (2:1, v/v), which had been determined as suitable for the coculture in preliminary experiments. At least three independent experimental runs were performed to evaluate each micro-biogeography.

After printing, we compared the microcosms printed using 1-, 3-, or 6-KSM elements at different time points using optical microscopy and plate counting techniques. In all of the scenarios analyzed, fluorescence signals in the micrographs decreased steadily over time (Figure 3A). Figure S1 depicts the fluorescence intensity of EcRFP in these bacterial microcosms. We further investigated this trend by assessing the viability of both EcRFP and LGG every 4 h by enumerating CFUs using the agar-plate method. As expected, the growth dynamics of both EcRFP and LGG were influenced by DSI (Figure 3B). The EcRFP viability decreased by the same proportion in all the printed microcosms during the first 4 h of cultivation. However, after 12 h the inhibition of EcRFP by LGG was less severe in the 1-KSM-fabricated constructs (DSI = 0.55 μm/μm) than in the 6-KSM-fabricated microcosms (DSI = 13.7 μm/μm; p-value < 0.01). This suggests that the lowest DSI was more favorable than the higher ones for EcRFP culture. Results suggest that the competition mechanisms of LGG, which were inactive or inefficient at the lowest DSI, were triggered at a higher degrees of intimacy with EcRFP, thereby inducing a stronger inhibition of this prey. In fact, the proximity of competitors has been suggested to regulate toxin secretion or inhibitors in bacterial communities.[8] We also conducted control experiments where *E. coli* and LGG were cultured independently or were mixed and cocultured in liquid or solid media (Figure S3). The results showed that LGG severely inhibits *E. coli* growth in well-mixed liquid cocultures (Figure S4A). For instance, LGG outgrows *E. coli* in mixed cultures in solid media and occupies 90% of the area of solid cocultures in 24 h (Figure S4B); however, no characteristic spatial patterns are distinguishable in these cultures. By contrast, chaotic bioprinting enables the fabrication and coculture of prede-signed structured communities with different DSI.

https://doi.org/10.1021/acsbiomaterials.0c01646
ACS Biomater. Sci. Eng. 2021, 7, 2408−2419

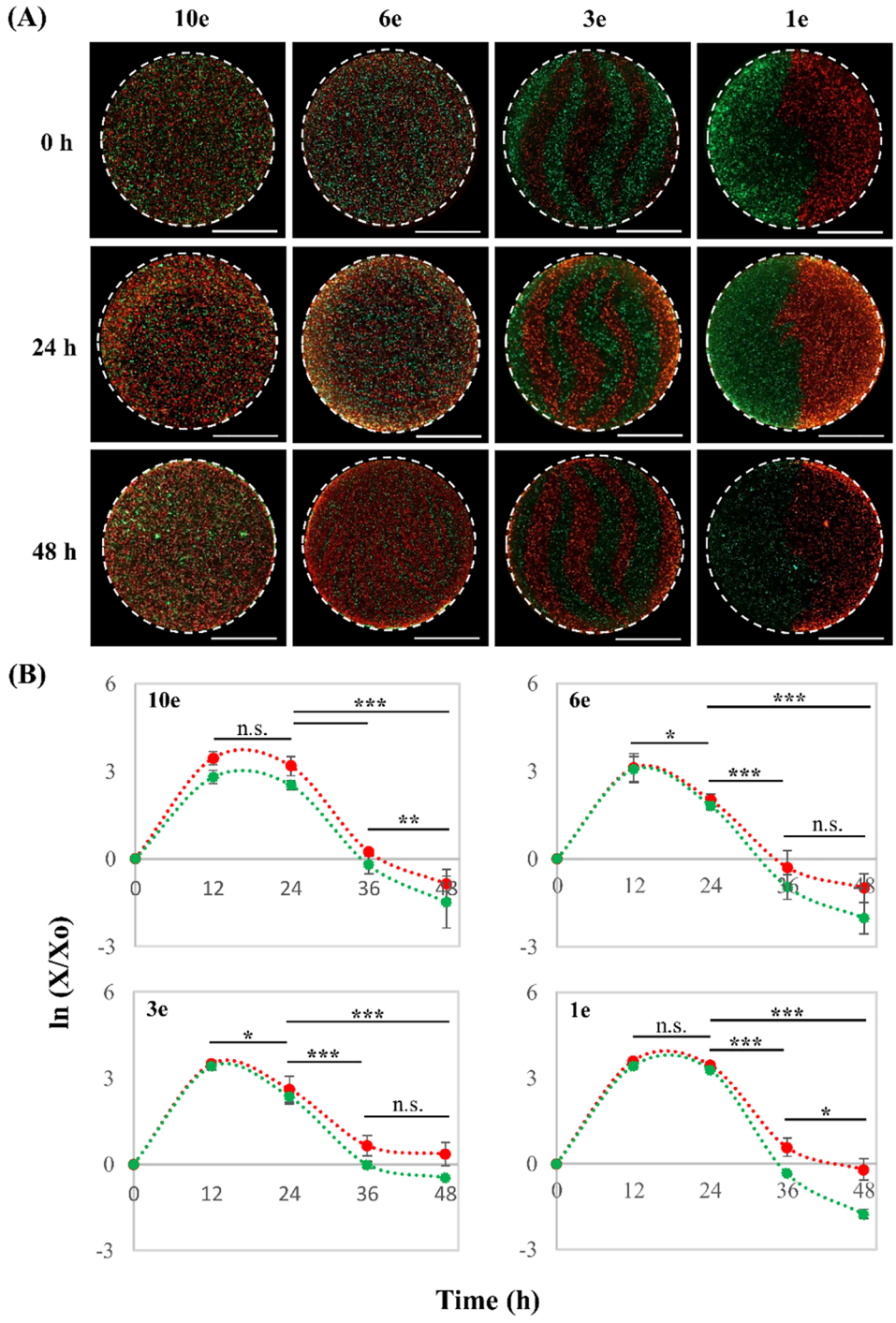

Figure 4. Growth dynamics of the *E. coli* consortia. (A) Cross-section of micro-biogeographies containing EcRFP (red) and EcGFP (green), chaotically bioprinted using 10-, 6-, 3-, or 1-KSM elements (scale bar: 500 μm). (B) Viability of EcRFP and EcGFP for 48 h, normalized by the number of CFUs just after bioprinting (X_0). One plot per micro-biogeography. *p-value < 0.05; **p-value < 0.001; ***p-value < 0.001 (n = 6).

Our observations are consistent with recent literature. Song et al.[40] assessed the capability of microencapsulated LGG to either disrupt or inhibit biofilms formed by *E. coli*. Exponential reduction of the biofilm was observed as early as 4 h of coculture. In addition, the authors found that the 3D-microenvironment stimulated the release of inhibitory molecules by LGG, thereby reducing the transcriptional activation of the *luxS* quorum-sensing pathway in *E. coli*. Analogous reports using the same prey (*E. coli*), but a different predator (i.e., *Bdellovibrio bacteriovorus*), have suggested that this bacterial species exhibits an enhanced persistence when its microcolonies are placed far away from its enemy and, in particular, at the periphery of the microlandscape.[41]

The dependency between DSI and bacterial competition can be explained in terms of mass transfer arguments. Bacteria use both contact-dependent and independent competition mechanisms.[42−44] In the first case, a bacterium secretes toxic substances directly into the cytoplasm of a member of a different species; contact is therefore mandatory and DSI is directly relevant. In the second case, bacteria secrete

https://doi.org/10.1021/acsbiomaterials.0c01646
ACS Biomater. Sci. Eng. 2021, 7, 2408−2419

specialized metabolites that diffuse into the microenvironment, where they interfere with the metabolism of susceptible microbial individuals. Distance is also relevant here since diffusion is inversely proportional to the square root of distance.[25] DSI is also highly relevant, since diffusive processes occur more effectively across structures with high perimeter-to-area ratios. Chemical and physical gradients at the local microenvironment play important roles in the dynamics of mixed bacterial communities, so they might influence gene expression and, consequently, growth dynamics.[10,45] Indeed, spatial distribution has been suggested as a key driver of gene expression due to the microscale concentration differences at distinct locations within a microbial consortium.[10,46,47]

Furthermore, spatial segmentation may mitigate the proliferation of specific bacterial species due to changes in local concentrations of signaling molecules.[36,48] Micro-biogeographies printed using a 1-KSM printhead provide only one frontier for competition allowing a safer establishment of microcolonies far away from the battlefront. Consequently, the survival outcome in this microcosm may be mainly influenced by the lethality of contact-independent weapons.

The fluorescence intensity in the 1-KSM-fabricated microcosms decreased near the shared border after 12 h (Figure 3A). In fact, Figure 3C,I shows that much of the EcRFP neighborhood (smooth layer showing small colonies; indicated with white arrows) was invaded by LGG (coarser layer). This trend was also observed in the micro-biogeographies printed using a 3-KSM printhead (Figure 3C II).

In addition, LGG experienced a stunted growth during the first 8 h when cocultured in 0.55 μm/μm DSI micro-biogeographies (fabricated using a 1-KSM printhead) when compared to growth in microcosms printed with 3- and 6-KSM printheads (p-value < 0.001). This trend was also noticed at 12 h (p-value < 0.05; p-value < 0.01). The lactate produced by LGG is also noxious itself.[49] High local concentration of this metabolite may have contributed to a slowing down of the proliferation of LGG since this lactate-producing strain was confined in a single lamella.

In conclusion, this probiotic−pathogen model scenario demonstrates that the inhibition dynamics was greatly dependent on the DSI between EcRFP and LGG. This finding may have relevant implications. A high number of viable LGG cells have been suggested to represent a determining factor in the effectiveness of medical interventions using this probiotic strain.[50] Therefore, studies that use LGG to suppress or control the growth of other microorganisms (i.e., those related to the activity of LGG against pathogenic bacteria) should consider that micro-biogeography may play paramount roles both in the inhibition dynamics of the prey and in the proliferation of LGG.

***E. coli* versus *E. coli*.** In our second proof-of-concept scenario, the same *E. coli* strain used above (EcRFP) was bioprinted with an *E. coli* strain that produced a green fluorescent protein (EcGFP). At first sight, and considering the similarity between the weapons of these two bacterial armies (both share practically the same genetic load), we would not expect any fierce competition between them. Indeed, the growth curves of monocultures of EcRFP and EcGFP are remarkably similar in control experiments performed using conventional culture techniques in liquid media (Figure S5A,I). However, various factors, such as limited space and resources, may lead to competition among bacterial strains, even within the same species,[8,9,51,52] if they exhibit slightly different specific growth rates. In particular, recombinant *E. coli* strains derived from the same original strain may exhibit different specific growth since the expression of different proteins is associated with different metabolic burdens.[53] Even differences in the plasmid copy number of two *E. coli* strains, producing the same recombinant protein, may lead to significant differences in growth rates.[52,54] Indeed, EcRFP grows statistically faster than EcGFP in liquid medium cocultures conducted by conventional methods (Figure S3A and S5A,II). Here, we challenged our biofabrication system to assess its usefulness to recapitulate these delicate dynamics.

In this set of experiments, we included a well-mixed microcosm printed using a 10-KSM element printhead in addition to the segregated microgeographies printed with 1-, 3- and 6-KSM elements. In all the printed micro-biogeographies, EcRFP and EcGFP exhibited increased fluorescence intensity from 0 to 12 or 24 h, and a subsequent decrease after 48 h of cultivation (Figure 4A). Figure S2 depicts the changes in fluorescence intensities for EcRFP and EcGFP over time. Moreover, the quantification of the total number of CFUs, using the agar-plate method, revealed that the cooperation/competition dynamics in the community was strongly influenced by the DSI between its members (Figure 4B). Figure 4 shows the time evolution of the populations of EcRFP and EcGFP, expressed as the natural logarithm $\ln(X/X_0)$, where the populations have been normalized with respect to the initial population of each strain (X_0). We observed a pronounced prevalence of EcRFP over EcGFP throughout cultivation in the 10-KSM-mediated microcosm, that is, the well-mixed micro-biogeography, (p-value < 0.001). Similarly, EcRFP significantly outcompetes EcGFP in cocultures performed on agar plates by conventional methods (Figure S3 and S5B), as EcRFP occupies more than 60% of the area of cocultures conducted on solid media after 24 h. In contrast, a sustained growth of both strains was observed in the segregated microgeographies. In the 6-KSM element printhead microcosm, both strains grew at equal proportions (Figure 4). Both, EcRFP and EcGFP reached a peak of growth at 12 h with an average magnitude similar to the highest viability of EcRFP in the well-mixed micro-biogeography (3.1 ± 0.1 and 3.4 ± 0.2 log units, respectively). Subsequently, both strains exhibited a death phase starting after 24 h of cultivation. In a similar fashion, when the microcosm was chaotically printed using 3-KSM elements, both EcRFP and EcGFP grew equitably and steadily for 12 h of cultivation and exhibited a death phase after 24 h. Nevertheless, the average peak of growth was higher in the consortium printed using 3-KSM elements than using 6-KSM elements (3.5 ± 0.1 vs 3.1 ± 0.1 log units, respectively).

This trend was also observed at 24 h in constructs printed using either 3- or 6-KSM elements (2.5 ± 0.2 and 1.9 ± 0.2 log units, respectively). Therefore, a smaller DSI (2.3 μm/μm) was more favorable for the coexistence of the *E. coli* strains than a larger DSI (13.7 μm/μm) in terms of growth dynamics.

Interestingly, in the micro-biogeography printed using 1-KSM element (0.55 μm/μm DSI), neither EcRFP nor EcGFP exhibited a death phase at 24 h. Instead, a continued stationary growth phase was evident (Figure 4B). The absence of a stationary growth phase in the 3-KSM- and 6-KSM-fabricated microcosms (Figure 4B) suggests that the depletion of substrate (or the production of inhibitory byproducts)

https://doi.org/10.1021/acsbiomaterials.0c01646
ACS Biomater. Sci. Eng. 2021, 7, 2408−2419

occurred sooner in these micro-biogeographies than in the fully segregated ones (printed using 1-KSM element).

In our system, the degree of competition among our segregated societies appears to be lower in segregated *E. coli* societies than in completely mixed microcosms. Our results are consistent with several recent reports that indicate a higher stability in partially segregated communities. For example, the creation of a single shared interface enabled the culture of two *E. coli* consortia for a longer time than when homogeneously mixed microenvironments were used.[55] *In silico* models have suggested that well-mixed microenvironments result in more complex interactions between *E. coli* strains than do segregated systems for supporting coexistence,[56] since individual bacteria sense genetic relatedness in their surrounding counterparts in order to establish or avoid cooperation.[57,58] Experimental data have also shown that harmonious coexistence between *E. coli* strains is disrupted in well-mixed microcosms.[59]

Our results also suggest that in segregated *E. coli*−*E. coli* microcosms the lowest DSI results in more stable microsystems. As more interfaces exist between the segregated regions, the long-term stability of the community is compromised. While societies fabricated using a printhead with 6-KSM elements reached their peak population in 12 h and then declined (p-value < 0.05), societies that shared 1 order of magnitude less interface reached a significantly higher population peak during the same time and remained a stable society for 12 additional hours. Note also that the rate of growth is significantly lower in the microcosms fabricated with 6-KSM elements than in the ones printed using 3 elements.

Overall, these results show that the condition where less competition occurs between both *E. coli* strains is the completely segregated scenario (fabricated using 1-KSM), followed by the partially segregated cases (where the growth curve of both strains are essentially similar but no stationary phase was achieved). The well-mixed case is the least favorable of all the scenarios explored. We conducted a new set of experiments where we monocultured and cocultured these *E. coli* strains in liquid and solid media using conventional microbiology techniques. Similarly, in these experiments the competition between both *E. coli* strains is evident in well-mixed coculture scenarios (Figure S5).

In silico models of *E. coli* have suggested that cells at the edge of a bacterial patch are in charge of expanding their territory boundaries, whereas cells at the interior play different roles, such as cross-feeding.[45] Therefore, the edges of the colony are zones of potential stress, where EcRFP and EcGFP compete to expand their territories.

We found that the growth dynamics in our *E. coli* consortium can be controlled by simply switching the DSI from 13.7 to 2.3 or to 0.55 μm/μm, thereby facilitating the emergence of a stationary growth phase whenever necessary. This straightforward approach may find powerful applications in bioproduction engineering and synthetic biology as segregated ecosystem diversity might make possible the synthesis of added-value compounds and highly complex materials even without redesigning metabolic pathways.[8,60,61]

CONCLUSIONS

In this study, we introduce continuous chaotic bacterial bioprinting as a practical and cost-effective tool to fabricate micro-biogeographies with an unprecedented resolution and throughput. To our knowledge, this is the first report that investigates the growth dynamics of microcosms composed of two microorganisms at a wide range of spatial scales, where the DSI is a key factor that defines competition or cooperation.

We present two series of proof-of-concept scenarios to show that this microfabrication technique is useful to create bacterial communities with controlled micro-biogeographies that derive in logical competition or cooperation outcomes. Continuous chaotic bioprinting may be an enabling platform in microbial ecology and related scientific fields that will allow the creation of spatially controlled living microsystems, which exhibit customizable degrees of segregation/interaction, at high printing resolution. Indeed, one strategy used to promote cooperation in a microbial consortium is to create segregation by controlling the spatial position of the microorganisms.[2,37,57,59] However, spatial patterning may not be suitable in specific cases, for example, when interstrain communication is required for efficient biosynthesis,[35] auxotrophy,[62] or gene transfer.[63]

We envision the utility of chaotic bacterial bioprinting for the development of customized microcosms in the analysis, for example, of the effects of micro-biogeography on the microbial transcriptome or gene transfer. We anticipate that this might have great relevance to the design of probiotic interventions and the understanding of the interplay between different species in complex ecosystems such as the gut, the oral cavity, or the skin. Implications of spatial segregation to phenomena such as antibiotic resistance[47,64] may be rigorously studied in chaotically bioprinted systems. Tailored design of microbial communities capable of orchestrating the synthesis of high-value molecules may also be an additional and attractive outcome of continuous chaotic bacterial bioprinting.

MATERIALS AND METHODS

Printing Setup. In general, our continuous chaotic printing system consisted of a commercial syringe pump Fusion 200 (Chemyx, Stafford, TX, U.S.A.) loaded with 5-mL sterile syringes, sterile plastic hoses, a disinfected printhead containing a specific number of KSM elements (Figure 1C,D), and a flask containing 2% aqueous $CaCl_2$ (Sigma-Aldrich, St. Louis, MO, U.S.A.). The KSM printheads were printed on a Form 2 SLA 3D printer (FormLabs, Somerville, MA, U.S.A.) using a standard resin (Clear FLGPCL04, FormLabs). We used the design parameters reported in our previous contribution[25] to establish a printhead outlet diameter of 1 mm. We used printheads with an internal diameter of 5.8 mm. The length and diameter of a single KSM element were 8.7 mm and 5.8 mm, respectively.

Bacterial Strains and Culture Conditions. We assessed the interaction between pairs of strains, namely an *E. coli* strain engineered to produce red fluorescent protein (EcRFP) and LGG (ATCC 53103) or a distinct *E. coli* strain engineered to produce green fluorescent protein (EcRFP). Using conventional microbiological methods, we first cultured pairs of strains (EcRFP and LGG or EcRFP and EcGFP) in liquid media (Figure S3A) in monoculture or coculture (Figure S3B). LGG (ATCC 53103) was grown in de Man, Rogosa, and Sharpe (MRS) medium (Merck, Darmstadt, Germany). A mixture of Luria−Bertani (LB) and MRS media (2:1, v/v) was used for the coculture of EcRFP and LGG in liquid media. This mix was determined to be suitable for the coculture in preliminary experiments. *E. coli* strains expressing either RFP or GFP were separately cultured in LB medium (Sigma-Aldrich) containing 1 μL/mL of chloramphenicol to retain the recombinant plasmid. We conducted conventional plate counting to determine the number of viable bacteria at different time points and produced growth curves for monoculture and coculture scenarios. For *E. coli* and LGG experiments in liquid media, differential counting was done by culturing in MRS or LB media. MRS medium supports the growth of LGG but not of *E. coli*. Conversely, LB medium is designed to cultivate recombinant *E. coli* strains but lacks some of the nutrients

https://doi.org/10.1021/acsbiomaterials.0c01646
ACS Biomater. Sci. Eng. 2021, 7, 2408−2419

required for the growth of LGG. In the case of EcRFP and EcGFP experiments, bacterial colonies were discriminated by the color of the fluorescent protein that they produce.

In additional control experiments conducted in solid media, EcRFP and LGG or EcRFP and EcGFP were first monocultured in liquid media for 12 h at 37 °C with shaking agitation at 100 rpm, mixed in equal proportions, and plated in solid media. The area coverage of each strain was determined using ImageJ software after 24 h of culture at 37 °C.

Bioink Preparation and Printing Experiments. Bacterial cultures were grown in distinct reservoirs for 24 h at 37 °C before printing experiments. *E. coli* strains expressing either RFP or GFP were separately cultured in LB medium (Sigma-Aldrich) containing 1 μL/mL of chloramphenicol to retain the recombinant plasmid. LGG (ATCC 53103) was grown in MRS medium (Merck, Darmstadt, Germany).

Bioinks were prepared following the following general protocol: approximately 10 mL of each bacterial culture was centrifuged at 8000 rpm for 10 min. The supernatant was discarded, and the pellet was resuspended in 2% sterile alginate solution (Sigma-Aldrich) supplemented with suitable culture medium (i.e., 2% LB broth for EcRFP or EcGFP, and 5.22% MRS broth for LGG).

In *E. coli* versus LGG experiments, the initial cell density of the bioinks, in terms of optical density, was adjusted to 0.025 and 0.1 absorbance units for LGG and EcRFP, respectively. In *E. coli* versus *E. coli* experiments, prior to the bioprinting process, both EcRFP and EcGFP were cultivated in fresh medium for 24 h. Pellets of the bacteria where suspended in sodium alginate, and the initial cell density of each bioink was adjusted to an optical density of 0.1, measured at 600 nm. Subsequently, each bioink was deposited in a distinct sterile syringe and connected to a KSM printhead. The bioinks were coextruded at a flow rate of 1.5 mL/min at room temperature while the printhead outlet was immersed in a 2% $CaCl_2$ solution. Bacteria-laden constructs were cultured in 6-well plates containing 3 mL of MRS-LB (1:2) medium for *E. coli* versus LGG micro-biogeographies or LB medium for *E. coli* versus *E. coli* experiments. All bioprinting experiments were performed aseptically inside a laminar flow cabinet, and the bacteria-laden fibers were cultivated in suitable growth media at 37 °C while shaking at 100 rpm.

The number of CFUs was assessed by disaggregating and homogenizing 0.1 g of sample in 0.9 mL of phosphate buffered saline (PBS). A 100 μL aliquot of homogenized sample was sequentially diluted in PBS. Sequential dilutions were seeded in duplicate on Petri dishes containing MRS-agar or LB-agar medium. The collected data was multiplied by the dilution factor and normalized by the initial number of CFU in constructs (i.e., viable cell count just after bioprinting). The results were depicted in logarithmic scale. Then, cell count over time was expressed as the ratio of the cell density (X) at each specific time point and the initial cell density (X_0). The magnitude of X is equal to X_0 at 0 h of cultivation; then, the natural logarithm ($\ln(X/X_0)$) is zero for every experimental treatment (Figure 3B). At least six independent constructs were analyzed at each time point.

Microscopy Analyses. For microscopy observation, the printed filaments were placed in 6-well plates loaded with 3 mL of culture medium per well. All of the samples were cultured at 37 °C with shaking at 100 rpm. At each time point of observation, filaments from at least two wells were transferred to Petri dishes containing PBS for subsequent imaging. Cross-sectional cuts (~500 μm in height) of the filaments were placed on a glass slide. Distilled water (3 μL) was then added on top of each sample to prevent dehydration. This procedure was repeated at each sampling time using filaments taken directly from the 6-well plates.

The microarchitecture and fluorescence of the chaotically printed fibers was assessed using an Axio Observer.Z1 microscope (Zeiss, Germany) equipped with Colibri.2 LED illumination and an Apotome.2 system (Zeiss). The channels used for fluorescence imaging were enhanced green fluorescent protein (EGFP) and carboxy-X-rhodamine (ROX) for capturing green and red signals, respectively. The fluorescence intensities and exposure times were 40% and 400 ms for the EGFP channel, and 60% and 800 ms for the ROX channel. A stitching algorithm, included in the microscope software (Zen Blue Edition, Zeiss), was used for producing wide-field micrographs.

Characterization of Microarchitecture. The DSI of each micro-biogeography was estimated according to eq 1. The measurements were performed using ImageJ software by Fiji. The results were expressed as the average of three independent micrographs per micro-biogeography (n = 3).

We evaluated the reproducibility of the lamellar microstructure by calculating the area of each black or red striation using ImageJ software. Once the scale bar was set, each lamella was surrounded using the freehand selection tool. The average of seven cross-sectional cuts (n = 7) was reported. In addition, the total area of either red or black lamellae in the cross-section was expressed as the sum of individual measurements.

Scanning Electron Microscopy (SEM). Scanning Electron Microscopy (SEM) images were obtained using a variable pressure scanning electron microscope EVO/MA25 (Zeiss). Briefly, printed fibers were sequentially incubated with 4% formaldehyde and 4% paraformaldehyde for 15 min each and then washed with PBS. The fibers were then successively dehydrated in an ethanol gradient (i.e., using 25, 50, 75, and 95% ethanol in water) for 1 h. The samples were then coated with gold and visualized at high vacuum mode.

Computational Simulation. Computational fluid dynamics simulation was implemented using ANSYS Fluent 2020 software. The 3D geometry of the system was discretized using a fine mesh of triangular elements, and a mesh refinement procedure was conducted to ensure convergence of results. Using this mesh, the Navier−Stokes equations of motion were solved at each node in laminar flow using a transient state implementation. A fluid density of 1000 kg m^{-3} and a viscosity of 0.1 kg m s^{-1} were used.[25,26] No-slip boundary conditions were imposed in the fluid flow simulations.

Statistical Analysis. All statistical analyses were performed using GraphPad Prism 8. Biological data were presented as the mean ± SD from at least six bacterial constructs (n = 6). On the basis of two-way analysis of variance (ANOVA) and Tukey multiple comparisons, differences between data were considered statistically significant at *p-value < 0.05, **p-value < 0.01, or ***p-value < 0.001.

■ ASSOCIATED CONTENT

Supporting Information

The Supporting Information is available free of charge at https://pubs.acs.org/doi/10.1021/acsbiomaterials.0c01646.

> Comparison of the surface area of analogous striations; fluorescence intensity (FI) of EcRFP in coculture with LGG for 12 h; FI of EcRFP and EcGFP in coculture for 48 h; schematic representation of the methodologies used to assess coculture growth in liquid and solid media; analysis of EcRFP-LGG growth in liquid and solid media; analysis of EcRFP-EcGFP growth dynamics in liquid and solid media (PDF)

■ AUTHOR INFORMATION

Corresponding Authors

Grissel Trujillo-de Santiago − *Centro de Biotecnología-FEMSA and Departamento de Ingeniería Mecatrónica y Eléctrica, Escuela de Ingeniería y Ciencias, Tecnologico de Monterrey, Monterrey, Nuevo Leon 64849, México;* orcid.org/0000-0001-9230-4607; Email: grissel@tec.mx

Mario Moisés Alvarez − *Centro de Biotecnología-FEMSA and Departamento de Bioingeniería, Escuela de Ingeniería y Ciencias, Tecnologico de Monterrey, Monterrey, Nuevo Leon 64849, México*; Email: mario.alvarez@tec.mx

Authors

Carlos Fernando Ceballos-González − *Centro de Biotecnología-FEMSA, Tecnologico de Monterrey, Monterrey, Nuevo Leon 64849, México*

Edna Johana Bolívar-Monsalve − *Centro de Biotecnología-FEMSA, Tecnologico de Monterrey, Monterrey, Nuevo Leon 64849, México*

Diego Alonso Quevedo-Moreno − *Departamento de Ingeniería Mecatrónica y Eléctrica, Escuela de Ingeniería y Ciencias, Tecnologico de Monterrey, Monterrey, Nuevo Leon 64849, México*

Li Lu Lam-Aguilar − *Centro de Biotecnología-FEMSA, Tecnologico de Monterrey, Monterrey, Nuevo Leon 64849, México*

Karen Ixchel Borrayo-Montaño − *Centro de Biotecnología-FEMSA, Tecnologico de Monterrey, Monterrey, Nuevo Leon 64849, México*

Juan F. Yee-de León − *Delee Corp., Mountain View, California 94041, United States;* orcid.org/0000-0001-6265-5596

Yu Shrike Zhang − *Division of Engineering in Medicine, Department of Medicine, Brigham and Women's Hospital, Harvard Medical School, Cambridge 02139, Massachusetts, United States*

Complete contact information is available at: https://pubs.acs.org/10.1021/acsbiomaterials.0c01646

Author Contributions

C.F.C.G., E.J.B.M., M.M.A., and G.T.d.S. designed the study. C.F.C.G. and E.J.B.M. analyzed the data. C.F.C.G., E.J.B.M., M.M.A., and G.T.d.S. wrote the manuscript. C.F.C.G., E.J.B.M., L.L.L.A., and K.I.B.M. performed all of the bacterial bioprinting experiments. D.A.Q.M. conducted all the computational simulations. C.F.C.G., E.J.B.M., and D.A.Q.M. prepared the illustrations. J.F.Y.d.L. fabricated the printheads by stereolithographic 3D printing. G.T.d.S., M.M.A., and Y.S.Z. edited the final versions of the manuscript. All of the authors read, commented on, and approved the manuscript.

Author Contributions

#C.F.C.G. and E.J.B.M. contributed equally to this work.

Notes

The authors declare no competing financial interest.

■ ACKNOWLEDGMENTS

C.F.C.G. and E.J.B.M. gratefully acknowledge financial support granted by CONACyT (Consejo Nacional de Ciencia y Tecnología, México) in the form of Graduate Program Scholarships. G.T.d.S. acknowledges the funding received from CONACyT, L'Oréal-UNESCO−CONACyT-AMC (National Fellowship for Women in Science, Mexico), and UC-MEXUS. M.M.A. acknowledges the funding received from the Biocodex Microbiota Foundation in México. M.M.A. and G.T.d.S. acknowledge funding provided from CONACyT. Y.S.Z. acknowledges the funding granted by the Brigham Research Institute. This research has been partially funded by the Tecnologico de Monterrey. We gratefully acknowledge the experimental contributions of Felipe López-Pacheco, Norma Alicia Garza-Flores, Carolina Chávez-Madero, Alan Roberto Márquez-Ipiña, and Everardo González-González to this work. We gratefully acknowledge the contribution of Carlos Ezio Garciaméndez Mijares in designing figures.

■ REFERENCES

(1) D'Souza, G. G. Phenotypic Variation in Spatially Structured Microbial Communities: Ecological Origins and Consequences. *Curr. Opin. Biotechnol.* **2020**, *62*, 220−227.

(2) Ben Said, S.; Tecon, R.; Borer, B.; Or, D. The Engineering of Spatially Linked Microbial Consortia − Potential and Perspectives. *Curr. Opin. Biotechnol.* **2020**, *62*, 137−145.

(3) Stacy, A.; McNally, L.; Darch, S. E.; Brown, S. P.; Whiteley, M. The Biogeography of Polymicrobial Infection. *Nat. Rev. Microbiol.* **2016**, *14*, 93−105.

(4) Tofalo, R.; Perpetuini, G.; Schirone, M.; Fasoli, G.; Aguzzi, I.; Corsetti, A.; Suzzi, G. Biogeographical Characterization of Saccharomyces Cerevisiae Wine Yeast by Molecular Methods. *Front. Microbiol.* **2013**, *4* (JUN), 1−13.

(5) Welch, J. L. M.; Dewhirst, F. E.; Borisy, G. G. Biogeography of the Oral Microbiome: The Site-Specialist Hypothesis. *Annu. Rev. Microbiol.* **2019**, *73*, 335−358.

(6) Klauck, G.; Serra, D. O.; Possling, A.; Hengge, R. Spatial Organization of Different Sigma Factor Activities and C-Di-GMP Signalling within the Three-Dimensional Landscape of a Bacterial Biofilm. *Open Biol.* **2018**, *8* (8), 180066.

(7) Aschenbrenner, I. A.; Cernava, T.; Erlacher, A.; Berg, G.; Grube, M. Differential Sharing and Distinct Co-Occurrence Networks among Spatially Close Bacterial Microbiota of Bark, Mosses and Lichens. *Mol. Ecol.* **2017**, *26* (10), 2826−2838.

(8) Nadell, C. D.; Drescher, K.; Foster, K. R. Spatial Structure, Cooperation and Competition in Biofilms. *Nat. Rev. Microbiol.* **2016**, *14*, 589.

(9) Yung-Hua, L.; Xiao-Lin, T. Quorum Sensing and Bacterial Social Interactions in Biofilms: Bacterial Cooperation and Competition. In *Stress and environmental regulation of gene expression and adaptation in bacteria*; Bruijn, F., Ed.; John Wiley & Sons, 2016; pp 1197−1205.

(10) Schreiber, F.; Ackermann, M. Environmental Drivers of Metabolic Heterogeneity in Clonal Microbial Populations. *Curr. Opin. Biotechnol.* **2020**, *62*, 202−211.

(11) Costello, E. K.; Lauber, C. L.; Hamady, M.; Fierer, N.; Gordon, J. I.; Knight, R. Bacterial Community Variation in Human Body Habitats across Space and Time. *Science (Washington, DC, U. S.)* **2009**, *326* (5960), 1694−1697.

(12) Proctor, D. M.; Fukuyama, J. A.; Loomer, P. M.; Armitage, G. C.; Lee, S. A.; Davis, N. M.; Ryder, M. I.; Holmes, S. P.; Relman, D. A. A Spatial Gradient of Bacterial Diversity in the Human Oral Cavity Shaped by Salivary Flow. *Nat. Commun.* **2018**, *9* (1), 681 DOI: 10.1038/s41467-018-02900-1.

(13) Welch, J. L. M.; Rossetti, B. J.; Rieken, C. W.; Dewhirst, F. E.; Borisy, G. G. Biogeography of a Human Oral Microbiome at the Micron Scale. *Proc. Natl. Acad. Sci. U. S. A.* **2016**, *113* (6), E791−E800.

(14) Dige, I.; Grønkjær, L.; Nyvad, B. Molecular Studies of the Structural Ecology of Natural Occlusal Caries. *Caries Res.* **2014**, *48* (5), 451−460.

(15) Proctor, D. M.; Shelef, K. M.; Gonzalez, A.; Davis, C. L.; Dethlefsen, L.; Burns, A. R.; Loomer, P. M.; Armitage, G. C.; Ryder, M. I.; Millman, M. E.; Knight, R.; Holmes, S. P.; Relman, D. A. Microbial Biogeography and Ecology of the Mouth and Implications for Periodontal Diseases. *Periodontology 2000* **2020**, *82*, 26−41.

(16) Donaldson, G. P.; Lee, S. M.; Mazmanian, S. K. Gut Biogeography of the Bacterial Microbiota. *Nat. Rev. Microbiol.* **2016**, *14*, 20−32.

(17) Li, D.; Chen, H.; Mao, B.; Yang, Q.; Zhao, J.; Gu, Z.; Zhang, H.; Chen, Y. Q.; Chen, W. Microbial Biogeography and Core Microbiota of the Rat Digestive Tract. *Sci. Rep.* **2017**, *7* (1), 1−16.

(18) Welch, J. L. M.; Hasegawa, Y.; McNulty, N. P.; Gordon, J. I.; Borisy, G. G. Spatial Organization of a Model 15-Member Human Gut Microbiota Established in Gnotobiotic Mice. *Proc. Natl. Acad. Sci. U. S. A.* **2017**, *114* (43), E9105−E9114.

(19) Cordero, O. X.; Datta, M. S. Microbial Interactions and Community Assembly at Microscales. *Curr. Opin. Microbiol.* **2016**, *31*, 227−234.

(20) Burmeister, A.; Hilgers, F.; Langner, A.; Westerwalbesloh, C.; Kerkhoff, Y.; Tenhaef, N.; Drepper, T.; Kohlheyer, D.; Von Lieres, E.; Noack, S.; Grünberger, A. A Microfluidic Co-Cultivation Platform to Investigate Microbial Interactions at Defined Microenvironments. *Lab Chip* **2019**, *19* (1), 98−110.
(21) Gude, S.; Pinçe, E.; Taute, K. M.; Seinen, A. B.; Shimizu, T. S.; Tans, S. J. Bacterial Coexistence Driven by Motility and Spatial Competition. *Nature* **2020**, *578* (7796), 588−592.
(22) Hynes, W. F.; Chacón, J.; Segrè, D.; Marx, C. J.; Cady, N. C.; Harcombe, W. R. Bioprinting Microbial Communities to Examine Interspecies Interactions in Time and Space. *Biomed. Phys. Eng. Express* **2018**, *4* (5), 055010.
(23) Chen, F.; Ricken, J.; Xu, D.; Wegner, S. V. Bacterial Photolithography: Patterning Escherichia Coli Biofilms with High Spatial Control Using Photocleavable Adhesion Molecules. *Adv. Biosyst.* **2019**, *3* (3), 1800269.
(24) Qian, F.; Zhu, C.; Knipe, J. M.; Ruelas, S.; Stolaroff, J. K.; Deotte, J. R.; Duoss, E. B.; Spadaccini, C. M.; Henard, C. A.; Guarnieri, M. T.; Baker, S. E. Direct Writing of Tunable Living Inks for Bioprocess Intensification. *Nano Lett.* **2019**, *19* (9), 5829−5835.
(25) Chávez-Madero, C.; de León-Derby, M. D.; Samandari, M.; Ceballos-González, C. F.; Bolívar-Monsalve, E. J.; Mendoza-Buenrostro, C.; Holmberg, S.; Garza-Flores, N. A.; Almajhadi, M. A.; González-Gamboa, I.; Yee-de León, J. F.; Martínez-Chapa, S. O.; Rodríguez, C. A.; Wickramasinghe, H. K.; Madou, M.; Dean, D.; Khademhosseini, A.; Zhang, Y. S.; Alvarez, M. M.; Trujillo-de Santiago, G. Using Chaotic Advection for Facile High-Throughput Fabrication of Ordered Multilayer Micro- and Nanostructures: Continuous Chaotic Printing. *Biofabrication* **2020**, *12* (3), No. 035023.
(26) Bolívar-Monsalve, E. J.; Ceballos-González, C. F.; Borrayo-Montaño, K. I.; Quevedo-Moreno, D. A.; Yee-de León, J. F.; Khademhosseini, A.; Weiss, P. S.; Alvarez, M. M.; Trujillo-de Santiago, G. Continuous Chaotic Bioprinting of Skeletal Muscle-like Constructs. *Bioprinting* **2021**, *21*, No. e00125.
(27) Hosseini Kakavandi, F.; Rahimi, M.; Jafari, O.; Azimi, N. Liquid−Liquid Two-Phase Mass Transfer in T-Type Micromixers with Different Junctions and Cylindrical Pits. *Chem. Eng. Process.* **2016**, *107*, 58−67.
(28) Nguyen, N. T.; Wu, Z. Micromixers - A Review. *J. Micromech. Microeng.* **2005**, *15*, R1.
(29) Hobbs, D. M.; Muzzio, F. J. The Kenics Static Mixer: A Three-Dimensional Chaotic Flow. *Chem. Eng. J.* **1997**, *67*, 153−166.
(30) Rosas-Flores, W.; Ramos-Ramírez, E. G.; Salazar-Montoya, J. A. Microencapsulation of Lactobacillus Helveticus and Lactobacillus Delbrueckii Using Alginate and Gellan Gum. *Carbohydr. Polym.* **2013**, *98* (1), 1011−1017.
(31) Allan-Wojtas, P.; Truelstrup Hansen, L.; Paulson, A. T. Microstructural Studies of Probiotic Bacteria-Loaded Alginate Microcapsules Using Standard Electron Microscopy Techniques and Anhydrous Fixation. *LWT - Food Sci. Technol.* **2008**, *41* (1), 101−108.
(32) Hobbs, D. M.; Alvarez, M. M.; Muzzio, F. J. Mixing in Globally Chaotic Flows: A Self-Similar Process. *Fractals* **1997**, *05* (3), 395.
(33) Alvarez, M. M.; Muzzio, F. J.; Cerbelli, S.; Adrover, A.; Giona, M. Self-Similar Spatiotemporal Structure of Intermaterial Boundaries in Chaotic Flows. *Phys. Rev. Lett.* **1998**, *81* (16), 3395−3398.
(34) Mukherjee, S.; Bassler, B. L. Bacterial Quorum Sensing in Complex and Dynamically Changing Environments. *Nat. Rev. Microbiol.* **2019**, *17*, 371−382.
(35) Alnahhas, R. N.; Winkle, J. J.; Hirning, A. J.; Karamched, B.; Ott, W.; Josić, K.; Bennett, M. R. Spatiotemporal Dynamics of Synthetic Microbial Consortia in Microfluidic Devices. *ACS Synth. Biol.* **2019**, *8* (9), 2051−2058.
(36) Hardy, L.; Cerca, N.; Jespers, V.; Vaneechoutte, M.; Crucitti, T. Bacterial Biofilms in the Vagina. *Res. Microbiol.* **2017**, *168* (9−10), 865−874.
(37) Johnston, T. G.; Yuan, S. F.; Wagner, J. M.; Yi, X.; Saha, A.; Smith, P.; Nelson, A.; Alper, H. S. Compartmentalized Microbes and Co-Cultures in Hydrogels for on-Demand Bioproduction and Preservation. *Nat. Commun.* **2020**, *11* (1), 563 DOI: 10.1038/s41467-020-14371-4.
(38) Segers, M. E.; Lebeer, S. Towards a Better Understanding of Lactobacillus Rhamnosus GG - Host Interactions. *Microb. Cell Fact.* **2014**, *13*, S7.
(39) Dhanani, A. S.; Gaudana, S. B.; Bagchi, T. The Ability of Lactobacillus Adhesin EF-Tu to Interfere with Pathogen Adhesion. *Eur. Food Res. Technol.* **2011**, *232* (5), 777−785.
(40) Song, H.; Zhang, J.; Qu, J.; Liu, J.; Yin, P.; Zhang, G.; Shang, D. Lactobacillus Rhamnosus GG Microcapsules Inhibit Escherichia Coli Biofilm Formation in Coculture. *Biotechnol. Lett.* **2019**, *41* (8−9), 1007−1014.
(41) Hol, F. J. H.; Rotem, O.; Jurkevitch, E.; Dekker, C.; Koster, D. A. Bacterial Predator−Prey Dynamics in Microscale Patchy Landscapes. *Proc. R. Soc. London, Ser. B* **2016**, *283* (1824), 20152154.
(42) Granato, E. T.; Meiller-Legrand, T. A.; Foster, K. R. The Evolution and Ecology of Bacterial Warfare. *Curr. Biol.* **2019**, *29*, R521−R537.
(43) Garcia, E. C. Contact-Dependent Interbacterial Toxins Deliver a Message. *Curr. Opin. Microbiol.* **2018**, *42*, 40−46.
(44) Stubbendieck, R. M.; Vargas-Bautista, C.; Straight, P. D. Bacterial Communities: Interactions to Scale. *Front. Microbiol.* **2016**, 1234 DOI: 10.3389/fmicb.2016.01234.
(45) Cole, J. A.; Kohler, L.; Hedhli, J.; Luthey-Schulten, Z. Spatially-Resolved Metabolic Cooperativity within Dense Bacterial Colonies. *BMC Syst. Biol.* **2015**, *9* (1), 1−17.
(46) Dal Co, A.; Ackermann, M.; Van Vliet, S. Metabolic Activity Affects the Response of Single Cells to a Nutrient Switch in Structured Populations. *J. R. Soc., Interface* **2019**, *16* (156), 20190182.
(47) Dal Co, A.; van Vliet, S.; Ackermann, M. Emergent Microscale Gradients Give Rise to Metabolic Cross-Feeding and Antibiotic Tolerance in Clonal Bacterial Populations. *Philos. Trans. R. Soc., B* **2019**, *374* (1786), 20190080.
(48) Werlang, C.; Cárcarmo-Oyarce, G.; Ribbeck, K. Engineering Mucus to Study and Influence the Microbiome. *Nature Reviews Materials* **2019**, *4*, 134−145.
(49) Jiang, Q.; Stamatova, I.; Kainulainen, V.; Korpela, R.; Meurman, J. H. Interactions between Lactobacillus Rhamnosus GG and Oral Micro-Organisms in an in Vitro Biofilm Model. *BMC Microbiol.* **2016**, *16* (1), 149 DOI: 10.1186/s12866-016-0759-7.
(50) Chen, W. *Lactic Acid Bacteria. Omics and Functional Evaluation.*; Chen, W., Ed.; Springer: Singapore, 2019.
(51) Nagy, K.; Sipos, O.; Gombai, É.; Kerényi, Á.; Valkai, S.; Ormos, P.; Galajda, P. Interaction of Bacterial Populations in Coupled Microchambers. In *Chemical and Biochemical Engineering Quarterly*; Assoc. of Chemists and Chemical Engineers of Croatia, 2014; Vol. *28*, pp 225−231.
(52) Wolfsberg, E.; Long, C. P.; Antoniewicz, M. R. Metabolism in Dense Microbial Colonies: 13 C Metabolic Flux Analysis of E. Coli Grown on Agar Identifies Two Distinct Cell Populations with Acetate Cross-Feeding. *Metab. Eng.* **2018**, *49*, 242−247.
(53) Li, Z.; Rinas, U. Recombinant Protein Production Associated Growth Inhibition Results Mainly from Transcription and Not from Translation. *Microb. Cell Fact.* **2020**, *19* (1), 1−11.
(54) Bentley, W. E.; Mirjalili, N.; Andersen, D. C.; Davis, R. H.; Kompala, D. S. Plasmid-Encoded Protein: The Principal Factor in the "Metabolic Burden" Associated with Recombinant Bacteria. Biotechnology Bioengineering, 1990. *Biotechnol. Bioeng.* **2009**, *102* (5), 1283−1297.
(55) Lehner, B. A. E.; Schmieden, D. T.; Meyer, A. S. A Straightforward Approach for 3D Bacterial Printing. *ACS Synth. Biol.* **2017**, *6* (7), 1124−1130.
(56) Ren, X.; Murray, R. M. Cooperation Enhances Robustness of Coexistence in Spatially Structured Consortia; *ECC, 18th European Control Conference*, Ed.; IEEE: Napoli, Italy, 2019.
(57) Cremer, J.; Melbinger, A.; Wienand, K.; Henriquez, T.; Jung, H.; Frey, E. Cooperation in Microbial Populations: Theory and Experimental Model Systems. *J. Mol. Biol.* **2019**, *431*, 4599−4644.

(58) Kraemer, S. A.; Wielgoss, S.; Fiegna, F.; Velicer, G. J. The Biogeography of Kin Discrimination across Microbial Neighbourhoods. *Mol. Ecol.* **2016**, *25* (19), 4875−4888.
(59) Kerr, B.; Riley, M. A.; Feldman, M. W.; Bohannan, B. J. M. Local Dispersal Promotes Biodiversity in a Real-Life Game of Rock-Paper-Scissors. *Nature* **2002**, *418* (6894), 171−174.
(60) Pande, S.; Merker, H.; Bohl, K.; Reichelt, M.; Schuster, S.; De Figueiredo, L. F.; Kaleta, C.; Kost, C. Fitness and Stability of Obligate Cross-Feeding Interactions That Emerge upon Gene Loss in Bacteria. *ISME J.* **2014**, *8* (5), 953−962.
(61) Patel, A.; Carlson, R. P.; Henson, M. A. In Silico Metabolic Design of Two-Strain Biofilm Systems Predicts Enhanced Biomass Production and Biochemical Synthesis. *Biotechnol. J.* **2019**, *14* (7), 1800511.
(62) Burmeister, A.; Hilgers, F.; Langner, A.; Westerwalbesloh, C.; Kerkhoff, Y.; Tenhaef, N.; Drepper, T.; Kohlheyer, D.; Von Lieres, E.; Noack, S.; Grünberger, A. A Microfluidic Co-Cultivation Platform to Investigate Microbial Interactions at Defined Microenvironments. *Lab Chip* **2019**, *19* (1), 98−110.
(63) Li, B.; Qiu, Y.; Song, Y.; Lin, H.; Yin, H. Dissecting Horizontal and Vertical Gene Transfer of Antibiotic Resistance Plasmid in Bacterial Community Using Microfluidics. *Environ. Int.* **2019**, *131*, 105007.
(64) Phalak, P.; Chen, J.; Carlson, R. P.; Henson, M. A. Metabolic Modeling of a Chronic Wound Biofilm Consortium Predicts Spatial Partitioning of Bacterial Species. *BMC Syst. Biol.* **2016**, *10* (1), 90 DOI: 10.1186/s12918-016-0334-8.

https://doi.org/10.1021/acsbiomaterials.0c01646
ACS Biomater. Sci. Eng. 2021, 7, 2408−2419